We are IntechOpen,
the world's leading publisher of
Open Access books
Built by scientists, for scientists

6,900
Open access books available

185,000
International authors and editors

200M
Downloads

154
Countries delivered to

Our authors are among the

TOP 1%
most cited scientists

12.2%
Contributors from top 500 universities

CLARIVATE ANALYTICS

BOOK
CITATION
INDEX

INDEXED

WEB OF SCIENCE™

Selection of our books indexed in the Book Citation Index
in Web of Science™ Core Collection (BKCI)

Interested in publishing with us?
Contact book.department@intechopen.com

Numbers displayed above are based on latest data collected.
For more information visit www.intechopen.com

Turbulence Diffusion Mechanism in Submerged Vegetation Flows

Michio Sanjou

Additional information is available at the end of the chapter

Abstract

Many aquatic plants are often observed, and the submerged canopy flow appears in natural rivers. Complex flow patterns such as Karman vortex and related coherent motions are formed behind vegetation. In particular, mass and momentum transfers and the vertical mixing process are promoted significantly between the within-canopy layer and over-canopy layer. Therefore, it is very important for river ecosystem to reveal turbulent diffusion in submerged vegetated open-channel flows. The present study conducted simultaneously PIV and laser-induced fluorescence (LIF) measurements using a pair of high-speed cameras to analyze the contribution of coherent vortex to the turbulent diffusion property.

Keywords: vegetation flows, turbulence, diffusion process

1. Introduction

Aquatic vegetation elements yield a complex current structure which consists of the within-canopy layer and the over-canopy layer. Streamwise velocity reduces within canopy in a submerged vegetation flows in which the water depth is larger than the vegetation height, and a relevant shear instability is generated in the vertical direction. This induces coherent turbulence events such as ejection and sweep; near a boundary zone includes the vegetation edge between the within-canopy and the over-canopy. It is therefore very important for preservation of an aquatic habitat and a river environment to reveal transport mechanisms of heat, mass, sediment concentration, and momentum in the vegetation edge. This chapter focused on fundamental hydrodynamic characteristics and related turbulent diffusion properties in the

vegetated open-channel flows, because the ejections and the sweeps may have significant relationship with the convection and diffusion of nutrition and suspended sediments.

Case	H (cm)	h (cm)	U_m (cm/s)	Fr	Re (×10⁴)
1	5.0	5.0	10.0	0.14	0.5
2	6.25			0.13	0.63
3	7.5			0.12	0.75
4	10.0			0.10	1.0
5	12.5			0.09	1.25
6	15.0			0.08	1.5
7	20.0			0.07	2.0

Table 1. Hydraulic condition varying relative water depth.

A turbulence structure in these canopy flows has been studied intensively in the meteorology. Raupach and Thom [1] have revealed velocity profiles and generation properties of turbulence energy by measurements of air tunnel with a roughness wall. Gao et al. [2] have conducted field measurements in deciduous forest and reported that the sweep and ejection motions influence heat transport significantly. Raupach et al. [3] have pointed out an analogy between the canopy-flow property and mixing-layer zone.

In contrast, river environmental problems arouse public interest recently, and thus, turbulence structure, mass, and momentum transport and their diffusion property of the vegetated open-channels have been highlighted. Nepf et al. [4] have proposed a diffusion model of dye concentration on the basis of random walk model, and they applied to the wake region behind an emergent plant model. Furthermore, Nepf [5] has revealed the relation between the turbulence. Sections 2 and 3 introduce turbulence structure in submerged vegetation flows and turbulent diffusion properties, respectively, on the basis of measurement results.

2. Turbulence structure in submerged vegetated flows

Hydrodynamic properties in vegetated canopy rivers, in which velocity distributions are largely changed in the vertical direction, are required to be revealed in hydraulic engineering. Specifically, the submergence depth, that is, the ratio of the water depth H to the vegetation height h, governs such hydrodynamics and coherent turbulent events significantly. There exists an outer layer in which the log-law layer is formed under high submergence condition, whereas, in the low submergence, the flow is directly influenced by the vegetation elements. Therefore, our research group conducted turbulence measurements in vegetated canopy open-channel flows by changing the relative submergence, and consequently, mean-flow properties, turbulence structure, and coherent motions were revealed as mentioned below.

2.1. Experimental method and hydrodynamic condition

The laboratory experiments were conducted in 10 m long and 40 cm wide tilting flume as shown in **Figure 1**. The plant models were composed of non-flexible strip plates and attached vertically on the bottom. The present plant model 50 mm height, 8 mm width, and 1 mm thickness. H is the water depth, and h is the vegetation height. L_v and B_v are the streamwise and spanwise spacings between neighboring elements, respectively. x, y, and z are the streamwise, vertical and spanwise coordinates. The vertical origin, $y = 0$, was chosen as the channel bed. The mean velocity components in each direction are defined as U, V, and W, the turbulent components are u, v, and w, respectively. For measurements of two components instantaneous velocity, that is, $\tilde{u}(t) \equiv U + u(t)$ and $\tilde{v}(t) \equiv V + v(t)$, within and above the canopy vegetation, a laser light sheet (LLS) was projected into the water vertically from the free-surface side. The LLS thickness is 2 mm thick, and it was generated by 2 W Ar-ion laser. The LLS was located at 7 m downstream from the inflow section. The illuminated images were taken by a CMOS camera (1000 × 1000 pixels) with 200 Hz frame rate and 60 s sampling time. The instantaneous velocity components in the vertical two-dimensional plane could be obtained by PIV algorithm. **Table 1** shows hydraulic cases. Seven kinds of hydraulic conditions were chosen by changing the relative submergence depth, that is, $H / h = 1.0$, 1.25, 1.5, 2.0, 2.5, 3.0, 4.0, and the bulk mean velocity was constant for these cases, that is, $U_m = 10$ cm/s.
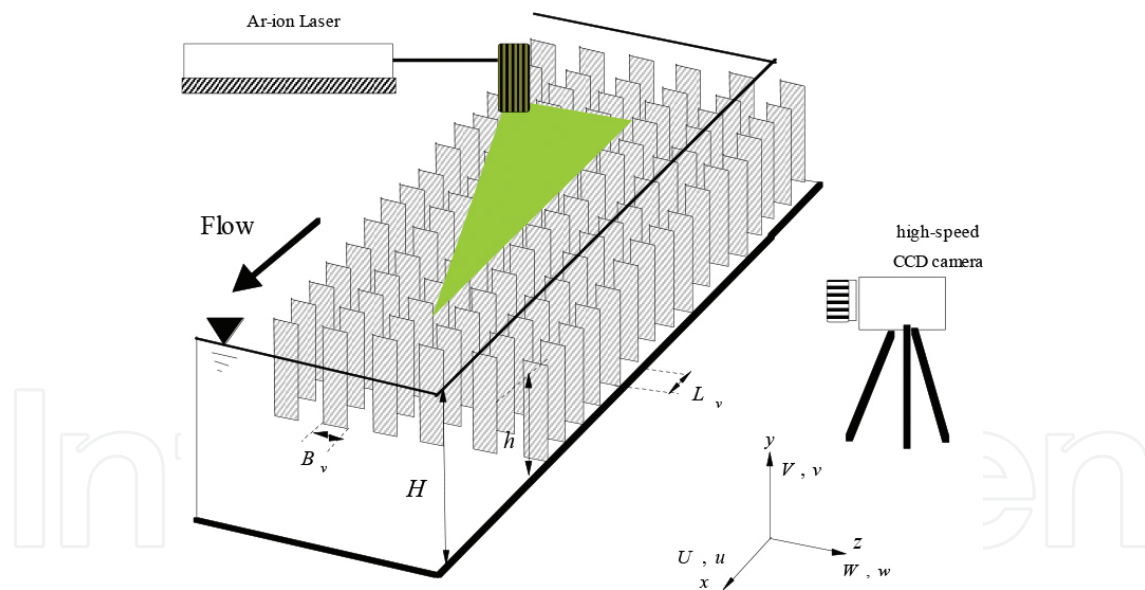

Figure 1. Experimental setup for PIV measurement in vegetated flume.

2.2. Mean flow structure

The whole depth region could be classified into two or three sublayers on the basis of the vertical profiles of mean streamwise velocity and Reynolds stress (see Poggi et al. [6]; Ghisalberti and Nepf [7]). Our research divides the vegetated open-channel flow into three sublayers as shown in **Figure 2**. The lowest layer within the canopy is termed the "wake zone (emergent

zone)," as defined by Nepf and Vivoni [8] and Ghisalberti and Nepf [7]. They defined the penetration depth h_p of momentum transfer, which is the upper limit of the wake zone and defined as the elevation of 10% of the maximum Reynolds stress. In the wake zone, the horizontal momentum transfer is dominated by stem wakes, and the vertical momentum transport is comparatively smaller than horizontal one. A middle sublayer includes the vegetation edge and is termed the "mixing-layer zone," which is characterized by the lower limit of h_p and the upper limit of h_{log}, which is defined later. The velocity profile has one inflection point near the canopy edge, and thus, the velocity fluctuations evolve to form large-scale coherent motions of sweeps and ejections, as pointed out by Raupach et al. [3]. The streamwise velocity profile obeys well the following log-law of rough boundary layers in a free surface layer termed the "log-law zone":
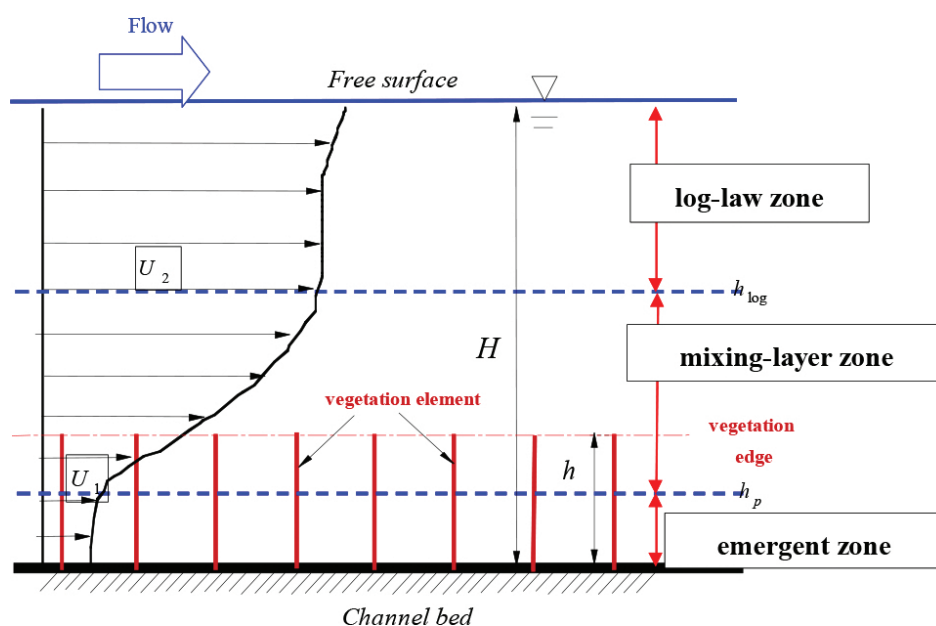

Figure 2. Classification of vertical layers in submerged vegetation flow.

$$\frac{U}{U_*} = \frac{1}{\kappa} \log\left(\frac{y-d}{y_0}\right)$$

(1)

in which, d and y_0 are the zero-plane displacement thickness and the roughness height, respectively. The von Karman constant κ was used as the standard value in the open-channel flows, that is, $\kappa = 0.412$ (Nezu and Nakagawa [9]). **Figure 3** shows the non-dimensional time-averaged velocity profiles for all submergence depth patterns. The results are normalized by the velocity at the vegetation edge, U_h layer is given by the following equationlayer is given by the following equation. A large velocity gradient $\partial U / \partial y$ is observed at the canopy edge, and in contrast, $\partial U / \partial y$ becomes smaller near the flume bed within-canopy. This is common tendency for all cases, irrespective of the submergence depth H/h. The velocity profiles

observed in the log-law zone, that is, $y \geq h_{\log}$, is recognized to coincide well with Eq. (1) in the large submergence depth of H / h =2.5, 3.0 and 4.0 as indicated in **Figure 4**.
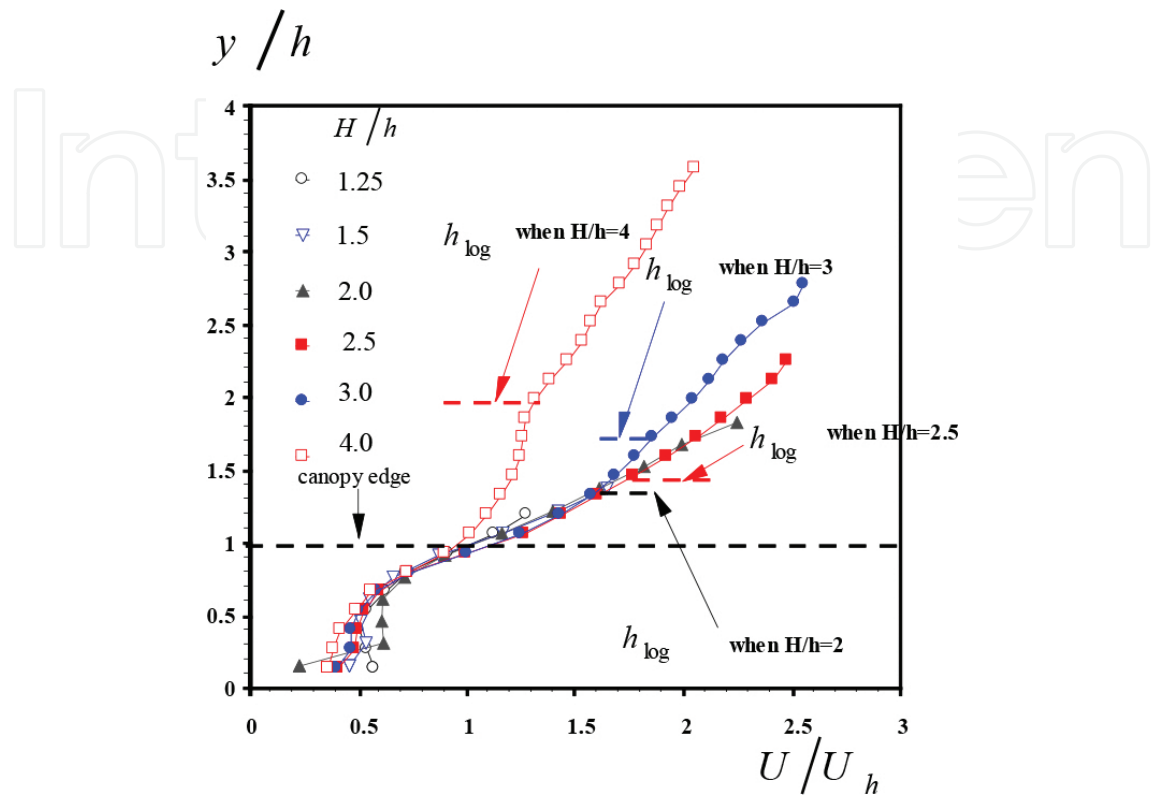
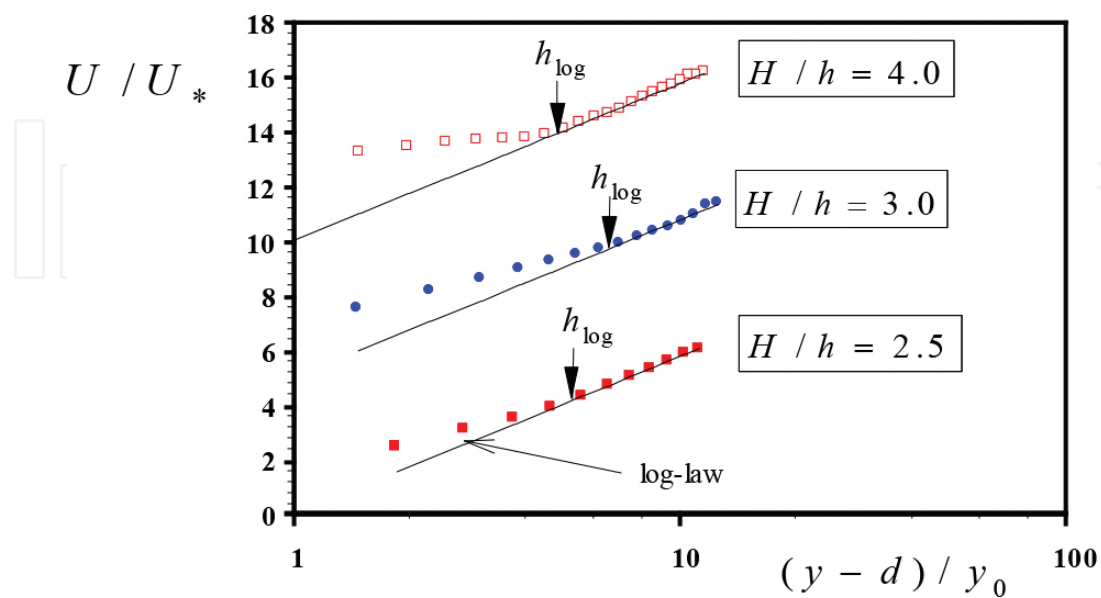**Figure 3.** Streamwise velocity profile normalized by outer variables.
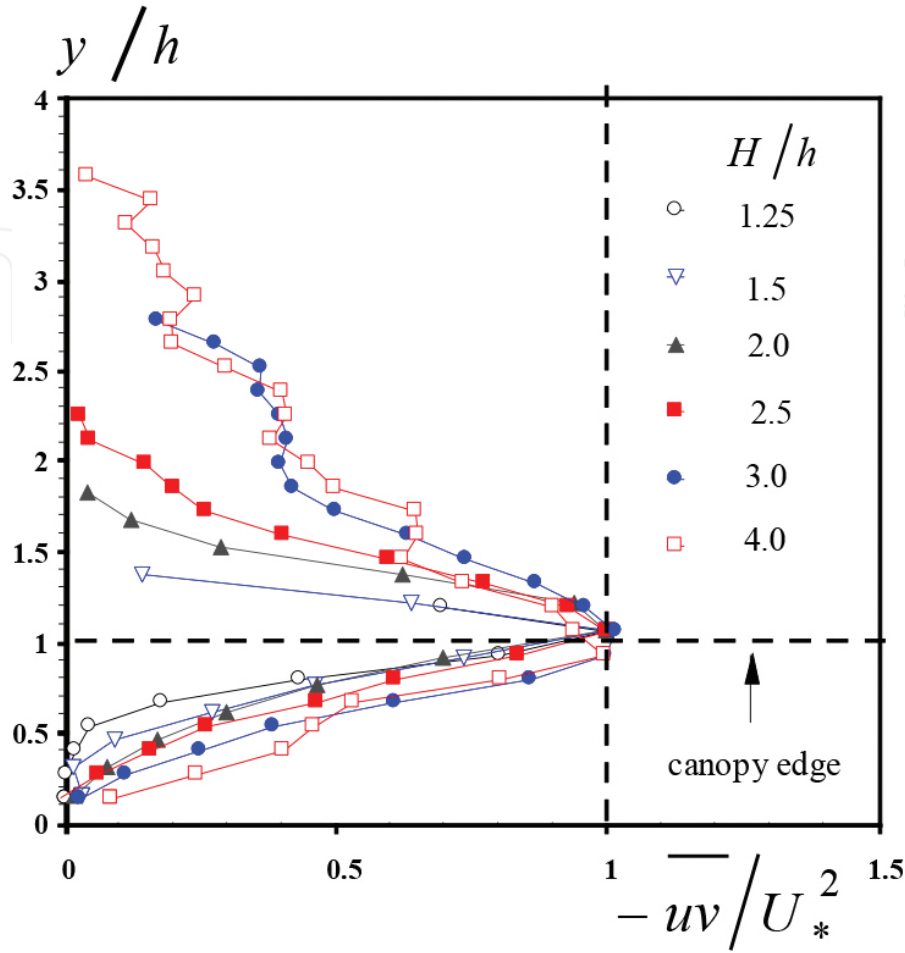
Figure 4. Examination of log-law over the canopy.

Figure 5. Reynolds stress profile.

Figure 5 shows the vertical profiles of Reynolds stress $-\overline{uv}$ normalized by the friction velocity U_*. The friction velocity could be evaluated as a peak value of $-\overline{uv}$. This result implies that $-\overline{uv}$ becomes larger within the canopy with an increase of the submergence depth. This suggests that the downward momentum transfer toward the within-canopy of $y < h$ is promoted more significantly as H/h increases. **Figure 6** shows the relationship between the penetration depth h_p and the submergence, in which previous other researchers' data in flexible canopy flows. The present result indicates that the penetration depth decreases with an increases of H/h in the same manner as pointed out by Nepf et al. [4] and Wilson et al. [10]. h_p becomes smaller in the present rigid canopy than in the flexible ones for the wide range of the submergence depth. This may be because the oscillations of flexible vegetations depressed the momentum transfer. The mean flow profile of mixing layer is given by the following equation.

$$\frac{U - \bar{U}}{\Delta U} = \frac{1}{2}\tanh\left(\frac{y - \bar{y}}{2\theta}\right)$$

(2)

in which, $\overline{U} = 1/2(U_1 + U_2)$, $\Delta U = U_2 - U_1$, $\overline{y} = (h_{\log} + h_p)/2$, and θ is the momentum thickness. U_1 is the constant velocity of the low-speed zone in mixing layer and corresponded to the velocity at $y = h_p$ in the present canopy-flow model (**Figure 2**).
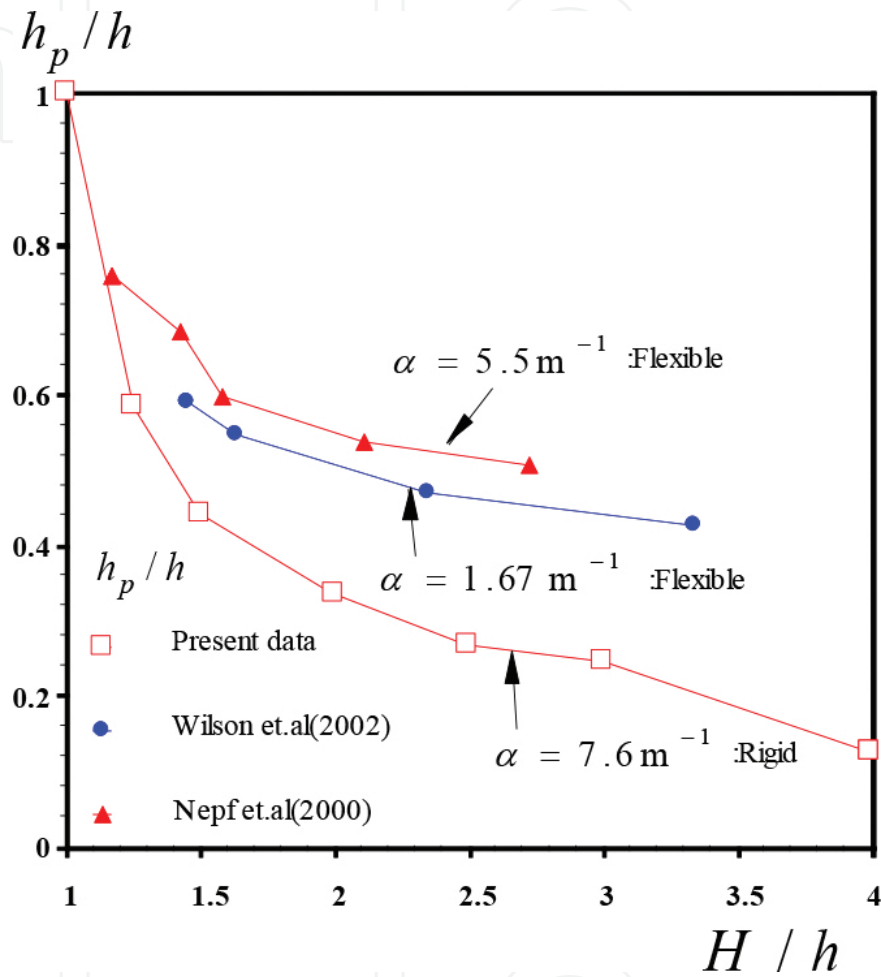

Figure 6. Relationship between the penetration depth and the relative depth.

U_2 is the constant velocity of the high-speed zone and assumed to be equal to the velocity at $y = h_{\log}$. **Figure 7** compares the mean flow profiles of the present canopy flow with the tangent hyperbolic curve of Eq. (2). In all cases, the present data are almost coincident with the Eq. (2) in the mixing-layer zone of $h_p < y < h_{\log}$. It is found that the width of the mixing-layer zone, that is, $\delta = h_{\log} - h_p$, becomes larger with an increase of H/h. In contrast, in the shallow submerged cases, $H/h = 1.25$ and 1.5, the discrepancies between the measured data and Eq. (2) are comparatively large, and consequently, the analogy between the canopy shear layer and the mixing layer becomes smaller.
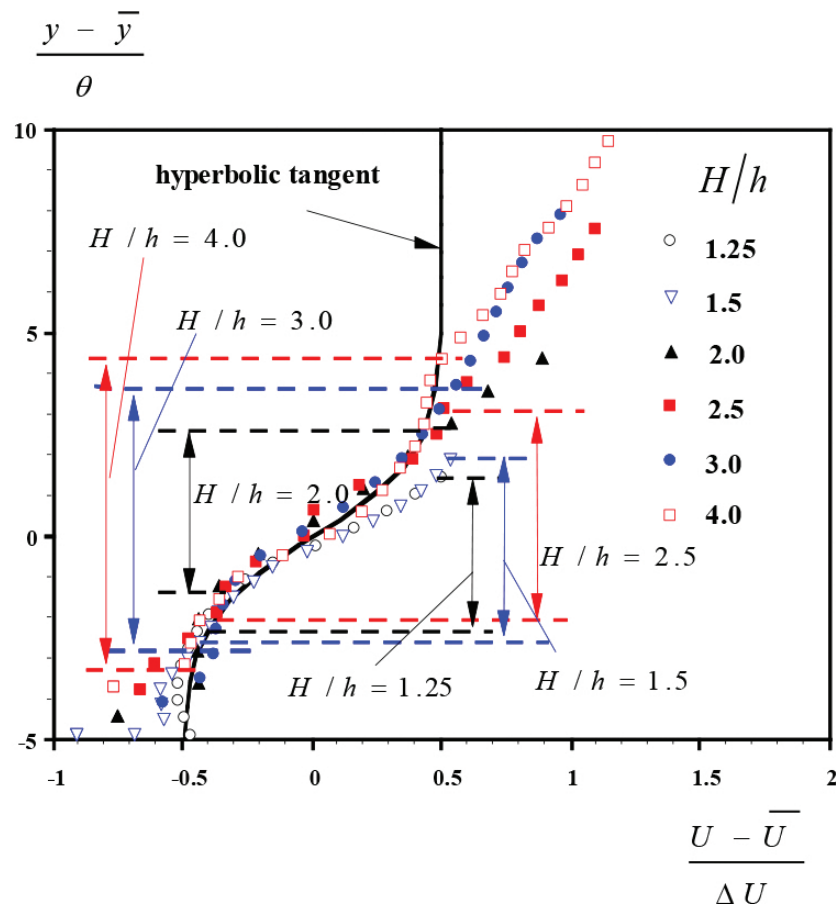
Figure 7. Examination of analogy with mixing layer.

2.3. Space–time analysis

Contours of space–time correlation between the streamwise velocity components, C_{uu}, are shown in **Figure 8**. C_{uu} is defined by as follows:

$$C_{uu} \equiv \frac{\overline{(\tilde{u}_0 - U_0) \times (\tilde{u}_{0+\Delta} - U_{0+\Delta})}}{u_0' \times u_{0+\Delta}'} \tag{3}$$

in which, the subscript 0 denotes a reference point, (x_0, y_0, z_0, t) and $0 + \Delta$ denotes a movable point $(x_0 + \Delta x, y_0 + \Delta y, z_0 + \Delta z, t + \tau)$. $u' \equiv \sqrt{\overline{u^2}}$ is the turbulence intensity, and the over-bar means the time-averaged operator. A large correlation-value zone is found to be transported downstream with an increase of the time lag τ, and thus an existence of mean coherent motions was recognized in **Figure 8**.

In the result of $\tau = 1.2$s, a trajectory line of the maximum correlation position was also shown at every 0.3 s. The vertical movement of the coherent motion is much smaller than the longitudinal one, and the coherent lump structure is moved in parallel to the horizontal canopy

plane. The convection velocity of mean eddies was evaluated from the distance between the maximum two-point correlation positions.
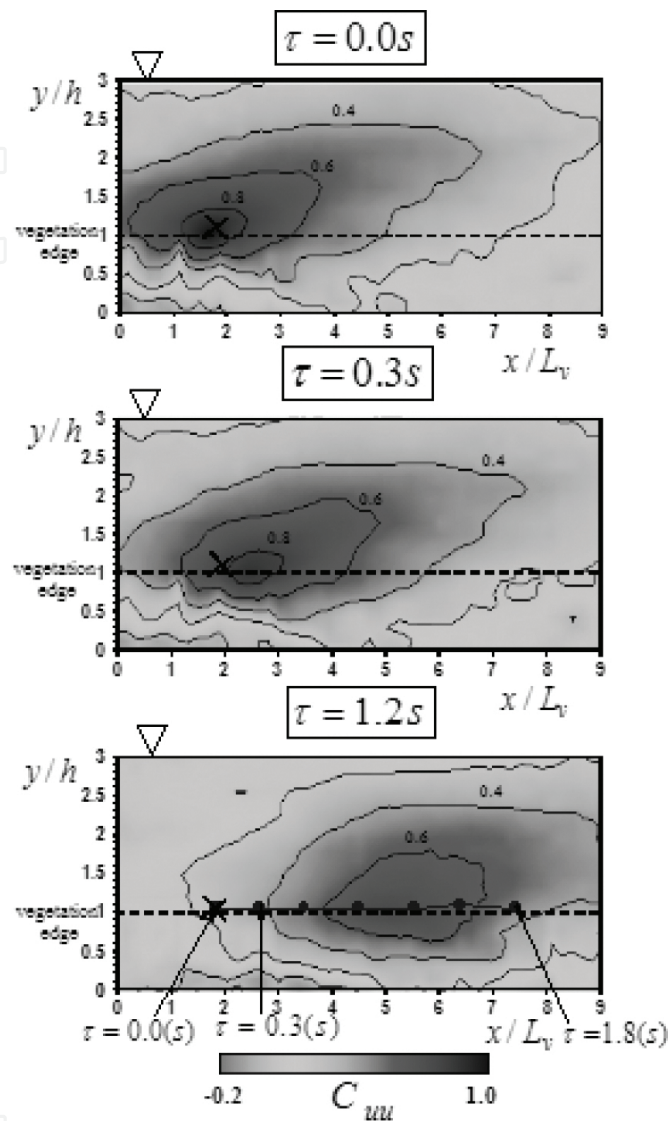

Figure 8. Space–time correlation property.

2.4. Visualization of coherent structure

Figure 9 shows time variation of the distributions of the instantaneous Reynolds stress $-uv$. In contrast, **Figure 10** shows the time series of the instantaneous velocity vectors, in which the contours of the streamwise velocity fluctuations $u(x, y, t)$ were also included. The time t indicated in **Figure 9** corresponds to that of **Figure 10** in order to compare the both figures each other. At $t = 0$ s, a large distribution of $-uv$ is observed locally, which is indicated by a dashed circle "A" in **Figure 9**. **Figure 10** suggests that the instantaneous velocity fluctuations are negative, $u < 0$, and thus, the upward vectors of the low-speed fluid are observed in the circle "A." That is to say, this zone forms a lump structure of the ejection motions. At $t = 0.36$

s, the ejection lump is convected downstream, and it is followed by the other local distribution of the dashed circle "B," which consists of a downward high-speed fluid, ($u > 0$ and $v < 0$), that is, a lump structure of the sweep motions. At $t = 0.96$ s, the ejections and sweeps are transported downstream. These results suggest that the local distributions of the high Reynolds stress correspond well to these lump structures of coherent motions. It was found from all digital frames that the sweeps and ejections seem to appear alternatively and periodically.

Periods of the sweeps and ejections, T_s and T_e, together with the period T_M of mixing layers are shown in **Figure 11**. T_M is a generation period of coherent eddies in pure mixing layer which is proposed theoretically by Ho and Huerre [11], as follows;

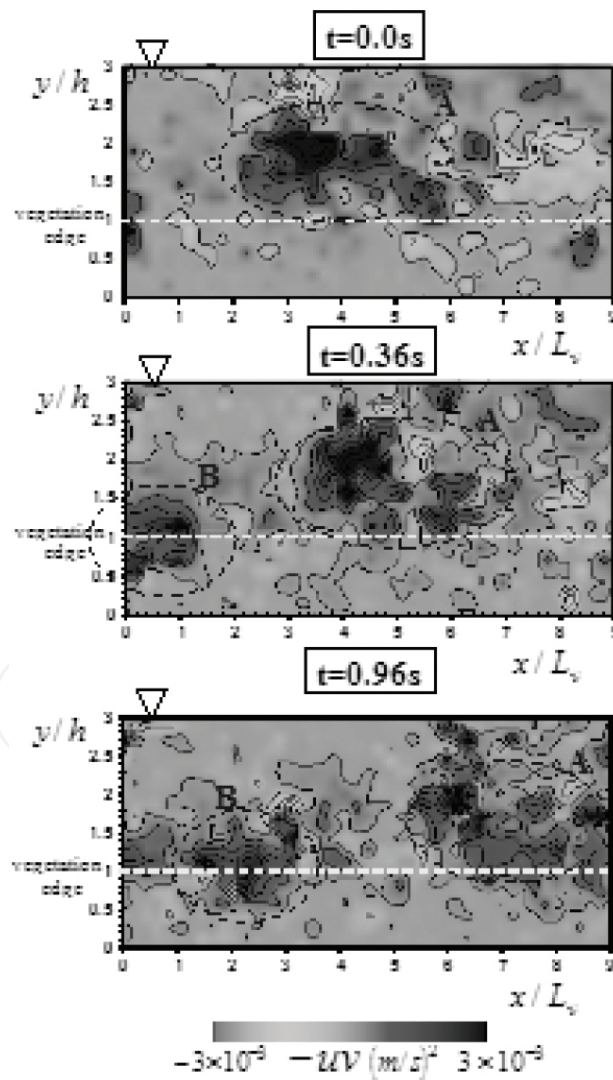$$T_M = \frac{\theta}{0.032\overline{\overline{U}}} \tag{4}$$

Figure 9. Instantaneous Reynolds stress.

T_S is almost same as T_E for all submergence cases, and they become larger with an increase of H/h, and this tendency is also observed in the theoretical value T_M. It is, therefore, found that the coherent motion of aquatic canopy flows resemble well that of mixing-layer flows, as pointed out for terrestrial canopy flows (see Raupach et al. [3]).
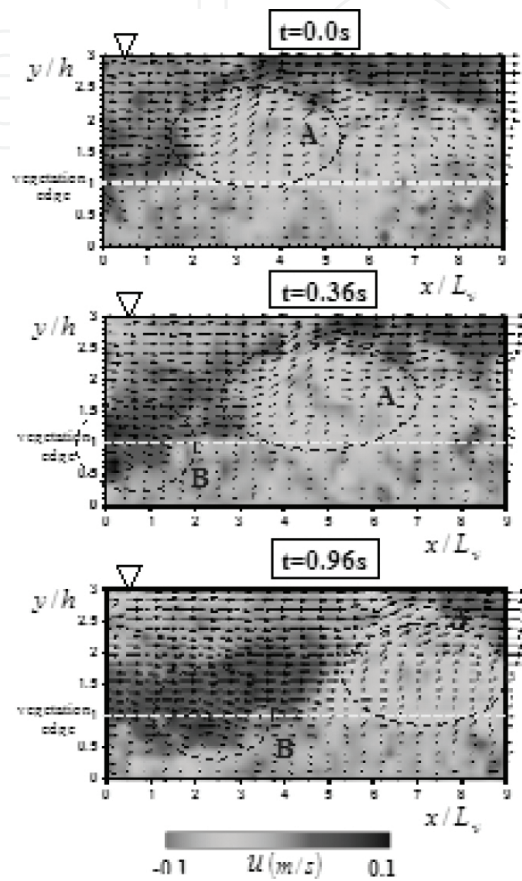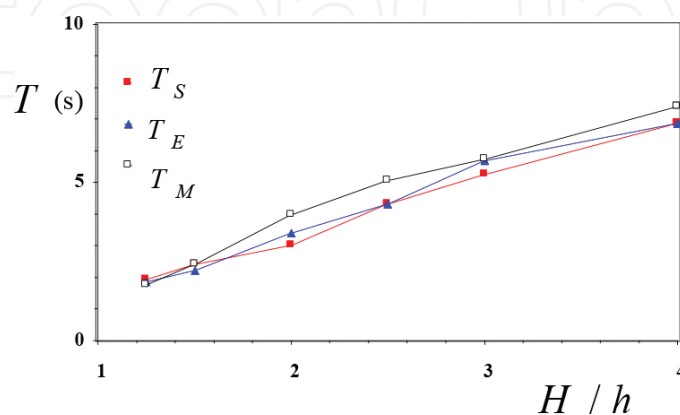

Figure 10. Instantaneous velocity vectors.

Figure 11. Periodicities of coherent events.

2.5. Detection of spanwise vortices

PIV measurements in turbulent boundary layers conducted by Adrian et al. [12] allow us to understand a packet structure of hairpin vortices. **Figure 12** shows same time-series of the instantaneous velocity vectors subtracted by a vortex convection velocity U_c near the vegetation edge. The convection velocity was evaluated from the space–time correlation analysis as mentioned before. **Figure 13** shows the distributions of the instantaneous vorticity $\Omega(x, y, t)$ at the same time as used in **Figure 12**. The time of these figures correspond to that of **Figures 9** and **10**. A vortex-like velocity-vector distribution appears in the ejection lump (the dashed circle of "A") at $t = 0$ s, and this lump is coincident with a large positive vorticity zone observed in **Figure 13**. This vortex-like structure is convected downstream at $t = 0.36$ s, and at the same time, vortex-like structure is also observed in the upstream region, which corresponds to the sweep zone of the dashed circle of "B." This sweep zone has a large positive vorticity as shown in **Figure 13**.
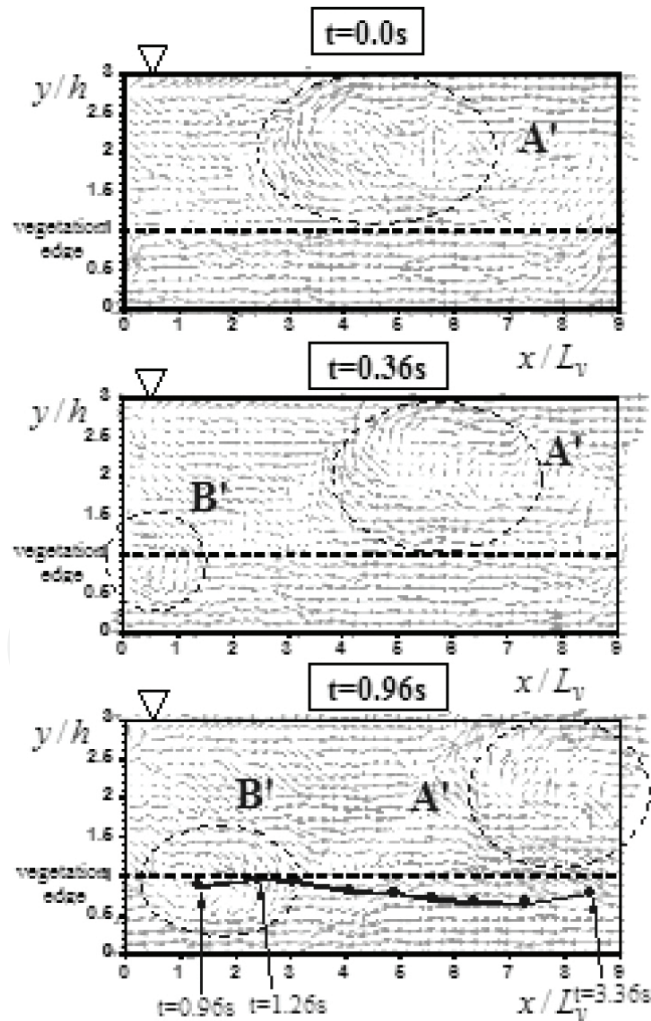

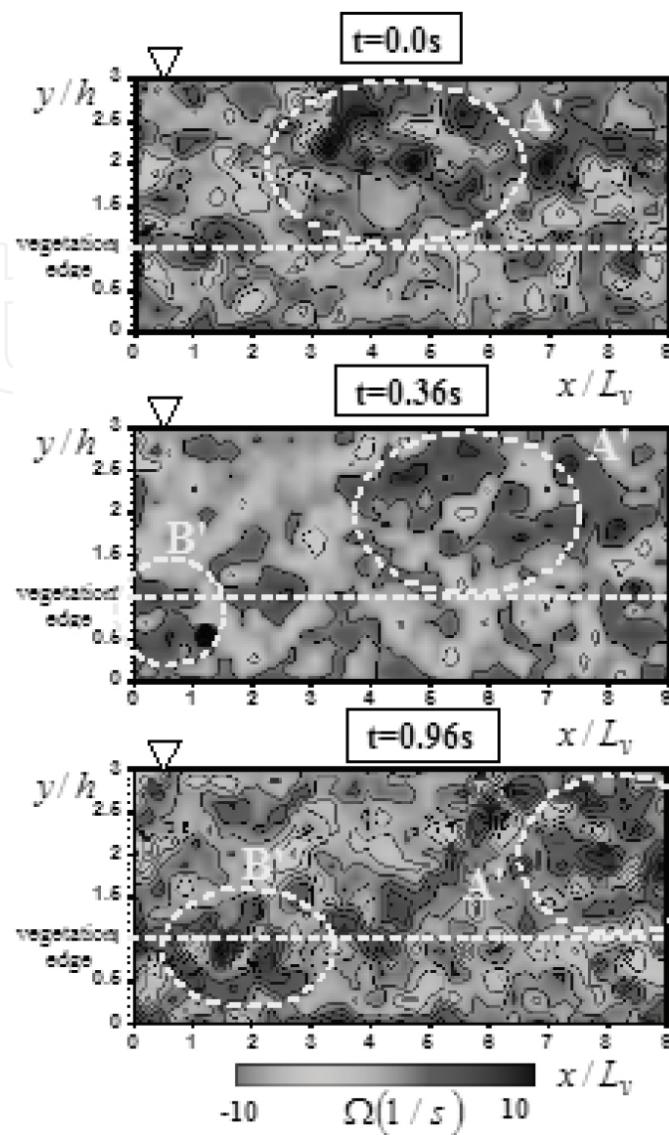**Figure 12.** Instantaneous velocity vectors.

Figure 13. Instantaneous vorticity distribution subtracted by eddy convection velocity.

Consequently, the ejections and sweeps form the organized coherent eddies. These coherent eddies are convected downstream at $t=0.96$ s. A trajectory line of core position of the coherent eddy "B" is also indicated at every 0.3 s in **Figure 12**. The vortex core was defined as the maximum position of the instantaneous vorticity Ω. The eddy observed near the vegetation edge at $t=0.96$ s. is transported into the within-canopy by the surrounding downward vectors, and this eddy exists within-canopy at $t=3.36$ s.

A length scale of the coherent eddy was evaluated accurately from the present PIV measured data in the following ways:

$$L_x \equiv \int_0^\infty \frac{\overline{u(x_0, y_0, t_0)u(x_0 + x, y_0, t_0)}}{u'(x_0, y_0)u'(x_0 + x, y_0)} dx \tag{5}$$

$$L_y \equiv \int_0^\infty \frac{\overline{u(x_0,y_0,t_0)u(x_0,y_0+y,t_0)}}{u'(x_0,y_0)u'(x_0,y_0+y)}dy \tag{6}$$

, in which L_x and L_y are the length scales for the streamwise and vertical directions. L_x is larger than L_y for all depth, and thus, it is found that oval-like vortices are generated near the vegetation edge. Both L_x and L_y are larger with an increase of H/h, and this suggests that large-scale vortices develop in the large submergence depth. In such a large submerged condition, the vertical length scale L_y has the same order of magnitude as the vegetation height, that is, $L_y \cong h$, as and indicated in **Figure 14**. Raupach et al. [3] reported the same tendency in the terrestrial canopies.
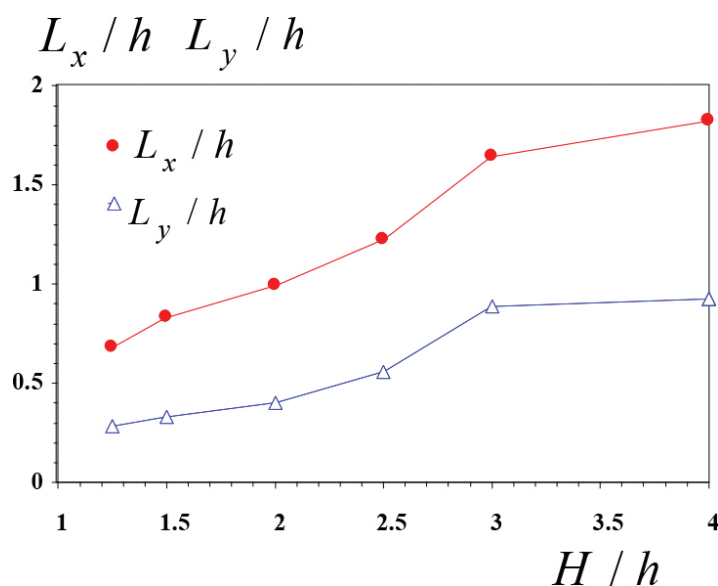

Figure 14. Relationship between the integral scales.

3. Turbulent diffusion in submerged vegetated canopy open-channel flows

Environmental problems in river basin have been recently highlighted as public interest, and thus, many researchers tried to reveal mass and momentum transfers associated with the wind waves, turbulence diffusion, and coherent vortex. Komori et al. [13] have revealed that wind waves promote gas transfer beneath air–water interface. There exists experimental works focused on the diffusion process in the vegetated canopies. Nepf et al. [4] have proposed a diffusion model of dye concentration on the basis of random walk model, and they applied it to the wake region behind an emergent plant model.

Furthermore, Nepf [5] has revealed the relation between the turbulence diffusion and the transport mechanism of dye concentration. However, there are many uncertainties about

turbulent diffusion mechanism, because it is hard to measure the velocity fluctuations and the concentration simultaneously. In consideration of this subject, our group tried to conduct some simultaneous measurements of PIV and the laser-induced fluorescence (LIF) using a pair of high-speed cameras, and evaluated the relation between the turbulent diffusion property and the coherent motions reasonably.

3.1. Experimental method

A schematic depiction of the turbulent diffusion in vegetated open-channel flows is shown in **Figure 15**. The shear instability occurs due to the velocity inflection point between the within-canopy and the over-canopy in the submergence condition as mentioned above. This instability causes the sweeps and ejections near the canopy edge, and these coherent motions have significant effects on mass and momentum exchanges between the within- and over-canopies. Concentration of sediment and nutrition are comparably large near the bottom bed in natural rivers, and these convection and diffusion processes are related significantly with activities of aquatic ecosystem. It is thus important to reveal the diffusion properties of turbulence in vegetated open-channel flows in order to promote such an environmental subject intensively.
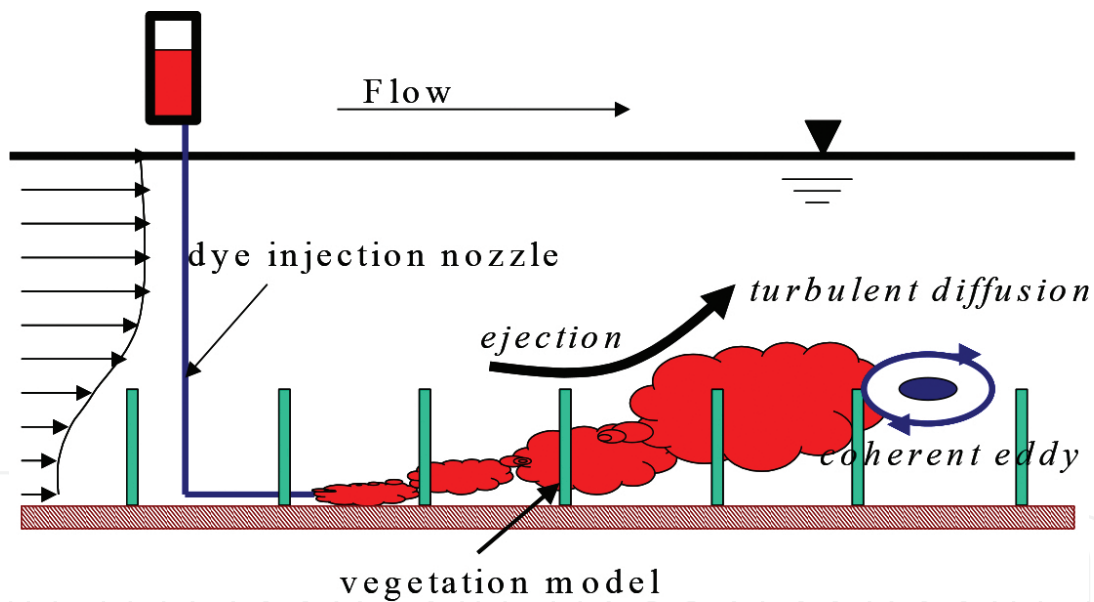

Figure 15. Sketch of developing vortices and turbulent diffusion.

The PIV-LIF measurement is introduced in this section. The contribution of turbulence structure to the diffusion process of the dye concentration is investigated by injecting dye near the flume bottom. Experiments were conducted in a 10 m long and 40 cm wide glass-wall flume. **Figure 16** shows the experimental setup and coordinate system. $\tilde{c} \equiv C + c$ is the instantaneous dye concentration, which is defined in the same manner as velocity components, that is, the Reynolds decomposition. H is the water depth, and h is the vegetation height. A vegetation element was made of $h \equiv 50$ mm non-flexible acrylic plate and 8 mm cubic base, in same manner as **Figure 1**.
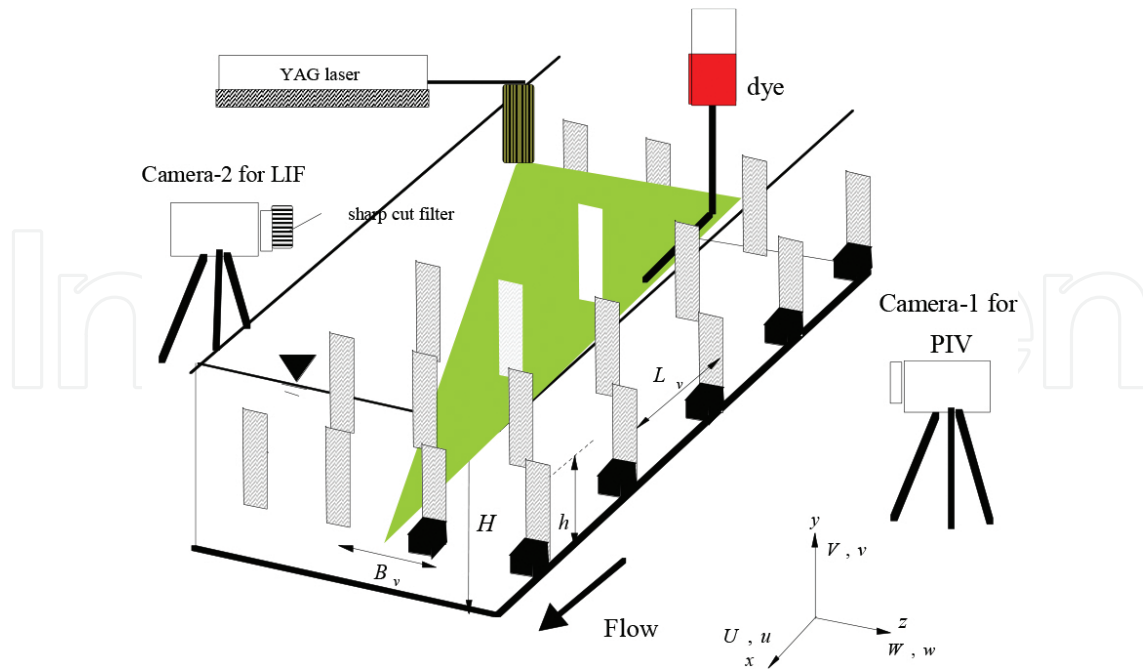
Figure 16. Experimental setup for PIV/LIF simultaneous measurement.

These vegetation models were placed vertically on the flume bed with a square grid allocation of $L_v = B_v = 24$ mm, in which L_v and B_v are streamwise and spanwise spacings between the neighboring plants, respectively. Dye (Rhodamine-B), the concentration of which was 0.1 g/l, was injected through a small stainless tube into the flow near the flume bed. The streamwise origin, $x = 0$, and the vertical origin, $y = 0$, were chosen as a tip of the injection nozzle and on the flume bed, respectively. The spanwise position of the injection nozzle was at the centerline of the non-wake region between the vegetation elements, which corresponds to the position of the laser light sheet (LLS) as mentioned later. The injection velocity of dye was controlled as coincident with the streamwise flow velocity at the same elevation. Two sets of high-speed CMOS cameras (1000 × 1000 pixels) were placed at both sides of the flume. One camera was used to PIV measurements, and the other was used to the LIF measurements. These cameras could be controlled simultaneously by using trigger signals of a pulse generator. 2 W YAG laser light sheet (LLS) was projected into the non-wake region, and the illuminated plane was taken by two sets of cameras with 200 Hz frame rate and 45 s sampling time. The time series of the instantaneous velocities ($\tilde{u}$, $\tilde{v}$) were obtained by the PIV algorithm. The reflection wavelength of the tracer particles is 537 nm (laser beam), In contrast, a fluorescence of dye induced by laser becomes a 580 nm wavelength. Therefore, it was possible that only the images of dye were taken by one CMOS camera using a sharp cutoff filter. The instantaneous distribution of the dye concentration was calculated from brightness values of the LIF images.

Table 2 shows the hydraulic condition. U_m is the bulk mean velocity, $\mathrm{Re} \equiv U_m H / v$ is the Reynolds number, and $Fr \equiv U_m / \sqrt{gH}$ is the Froude number. In this study, the emergent case ($H/h = 0.9$) was also conducted in order to consider the effects of the submergence depth on

turbulent diffusion. The bulk mean velocity of the emergent vegetation case was the same as that of the within-canopy zone measured in the submerged case. λ is the vegetation density.

Case	H/h	U_m (cm/s)	H (cm)	Re	Fr	h (cm)	λ
Submerged	3.0	10.0	15	15,000	0.08	5.0	0.39
Emergent	0.9	4.2	4.5	1890	0.06		

Table 2. Hydraulic condition for PIV/LIF experiments.

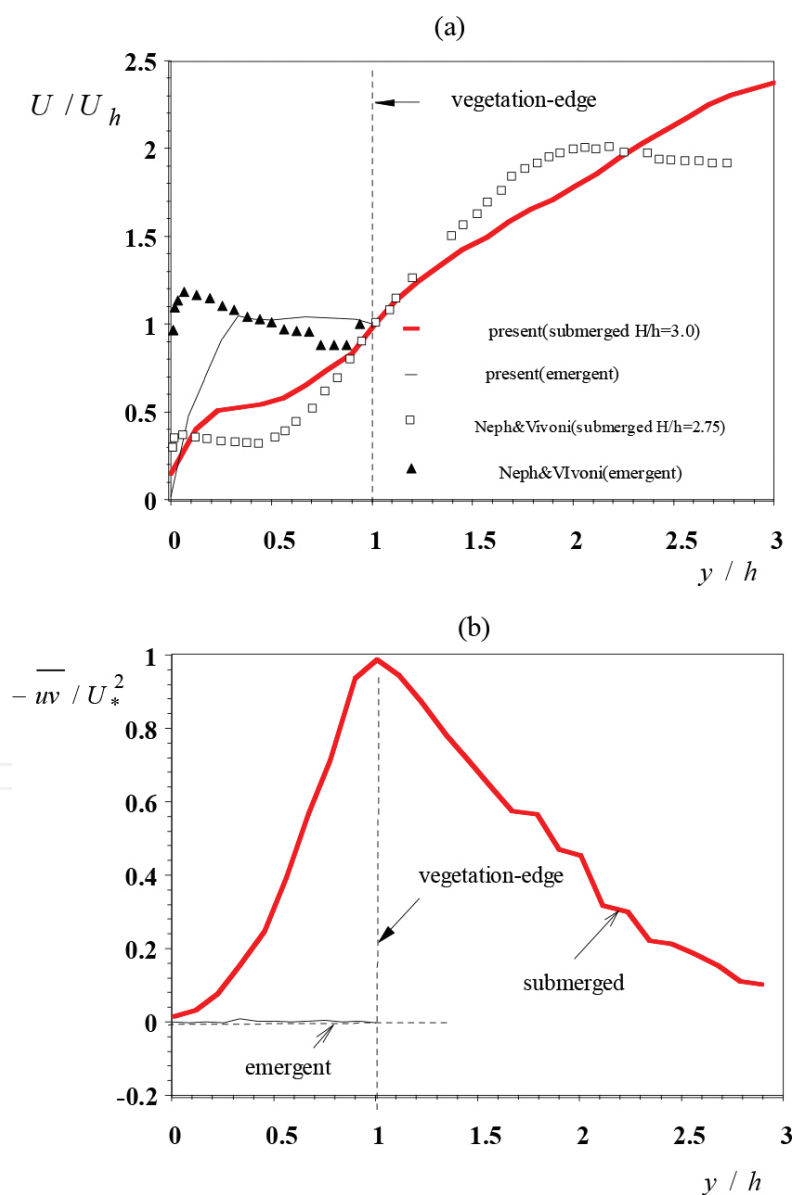## 3.2. Basic characteristics of flow structure

Figure 17. Vertical profiles of time-averaged velocity and Reynolds stress. (a) Mean velocity, (b) Reynolds stress.

Figure 17a, **b** shows the vertical profiles of time-averaged primary velocity $U(y)$ and Reynolds stress $-\overline{uv}$, respectively. The value of U was normalized by the velocity at the vegetation edge, U_h. The friction velocity U_* is defined as the value of $-\overline{uv}$ at the vegetation edge, $y/h = 1$. In the submerged case, the velocity profile $U(y)$ seems to resemble a mixing-layer type, in which the velocity difference is seen remarkably between the within-canopy and the over-canopy. Consequently, a typical shear layer is formed between them and coherent motions such sweeps and ejections are generated near the canopy edge. Although there are some discrepancies between the present data and Nepf and Vivoni's data, the same tendency is obtained in both data. Nepf and Vivoni suggested that the velocity dip phenomenon appears near the free surface, at $y/h = 2$. This may be because secondary currents are generated due to the small aspect ratio of their flume experiments. Reynolds stress $-\overline{uv}$ is recognized to have maximum at $y/h = 1$, and this implies that the momentum exchanges are promoted significantly by the velocity shear shown in **Figure 17a**.

In the emergent case, $U(y)$ is almost constant except for the near-bed region in both of the present data and Nepf and Vivoni's data. $-\overline{uv}$ becomes negligibly small in comparison with the submerged case. It is considered that the vertical momentum transport is negligibly small in the emergent vegetation.
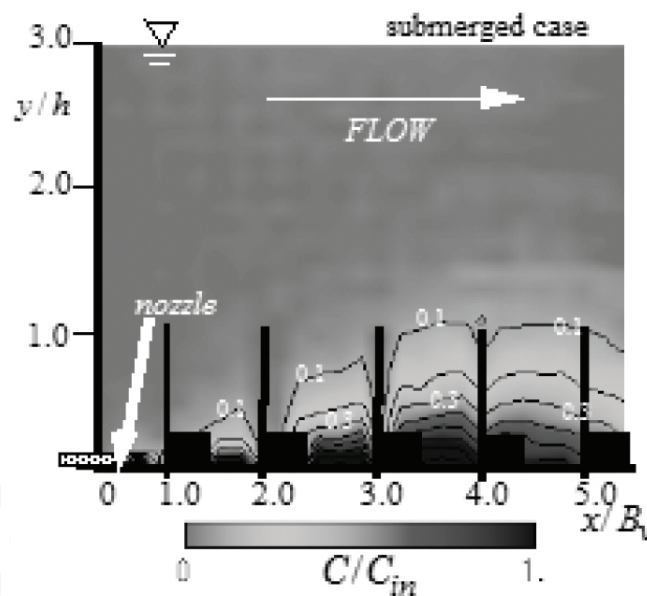

Figure 18. Distribution of time-averaged dye concentration.

3.3. Time-averaged dye concentration

The distribution of time-averaged concentration $C(x, y)$ is shown in **Figure 18** in which the contour values are normalized by the time-averaged concentration at the nozzle tip C_{in}. The dye concentration is observed to be transported in the streamwise direction, associated with the vertical diffusion. **Figure 19a** shows the vertical profile of C/C_{bed}, in which C_{bed} is the time-averaged concentration at the first measurement point very near the flume bed, $y/h = 0.06$.

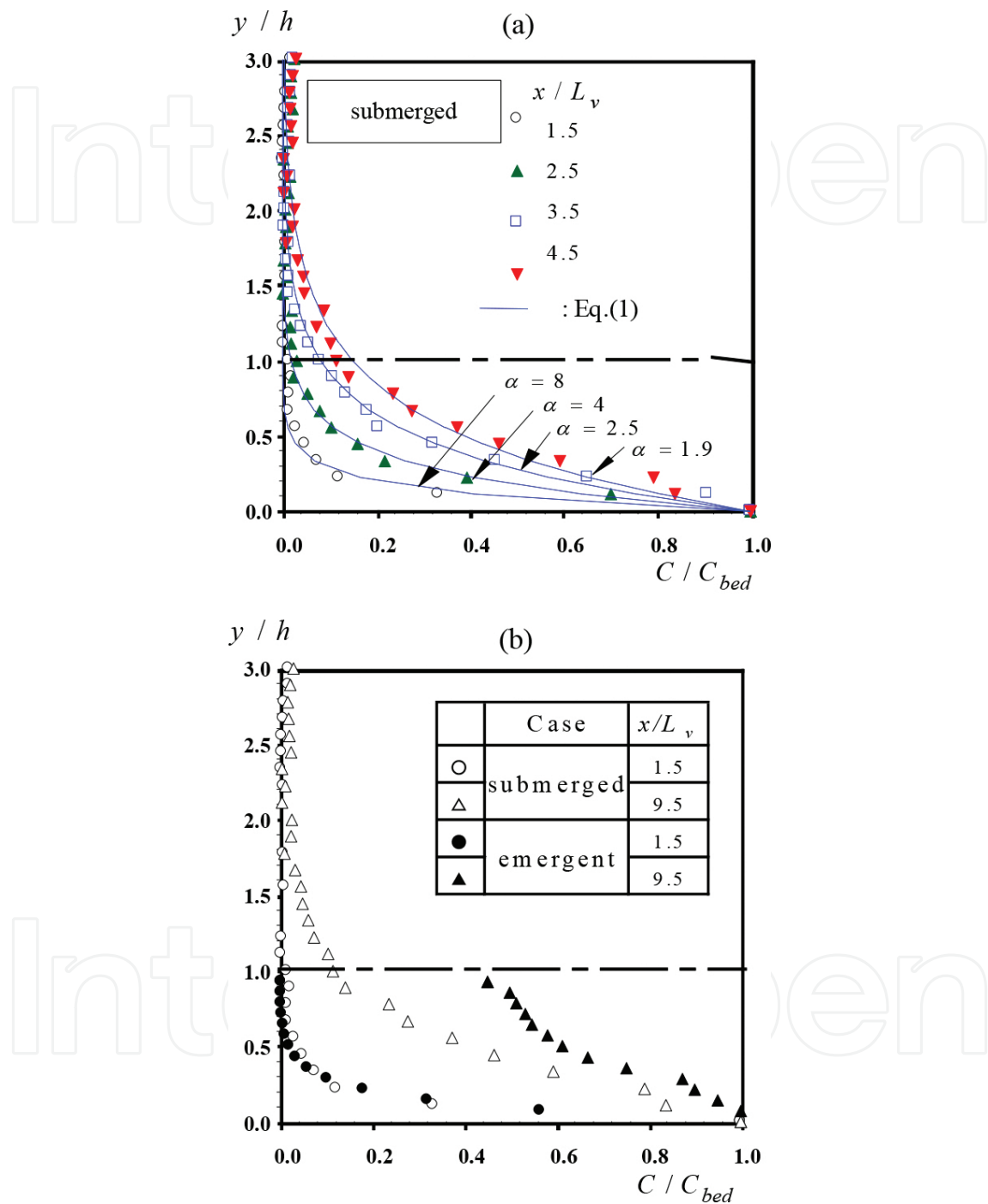These profiles can be described well by the following exponential function at every longitudinal position.

Figure 19. Vertical profiles of time-averaged concentration. (a) For submerged cases, (b) comparison of submerged and emergent cases.

Figure 19b shows some comparisons between the submerged and the emergent cases. The concentration is larger within the canopy at x/L_v=9.5 in the emergent case than in the

submerged case. This implies that the streamwise exchanges are conducted more significantly in emergent than submerged vegetation. **Figure 20** shows the streamwise variation of the diffusion width δ. It is defined as the elevation at which $C = 1/2\ C_{bed}$ (a half-value width). δ increases more linearly in the emergent than in the submerged cases. In contrast, in the submerged case, δ increases mildly at $x/L_v > 4$ and attains constant downstream of $x/L_v > 7$.
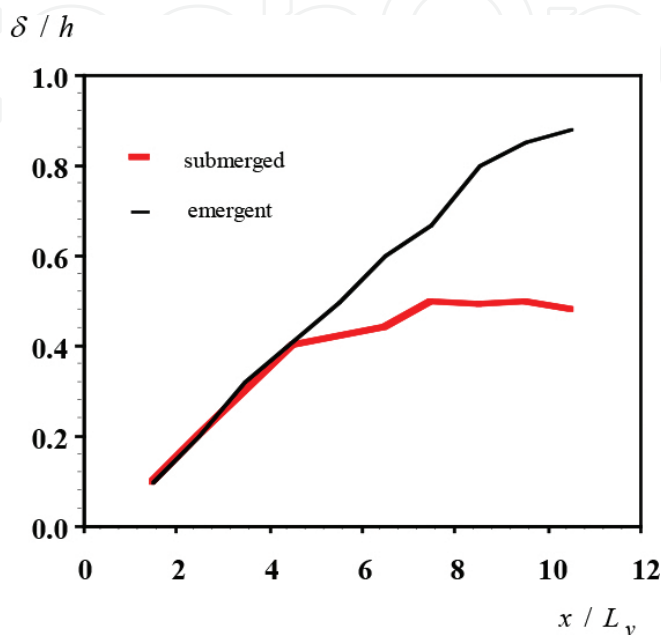

Figure 20. Longitudinal variation of diffusion width.

3.4. Evaluation of turbulent diffusivity

Reynolds stress and the correlation $\overline{vc}$ between the velocity and concentration are connected to be the following forms by the gradient diffusion model.

$$-\overline{uv} = v_t \partial U / \partial y \tag{7}$$

$$-\overline{vc} = K_y \partial C / \partial y \tag{8}$$

in which v_t is the eddy viscosity, and K_y is the turbulent diffusivity in the vertical direction. **Figure 21** shows the vertical profiles of v_t and K_y evaluated from Eqs. (7) and (8). K_y increases from the within-canopy to the canopy-edge zone, and decreases in the free surface region of $y/h > 2$. It has a peak value over the canopy of $1 < y/h < 2$. The profile of K_y resembles that of v_t. Therefore, it is considered that K_y is nearly equal to v_t in the vegetation-edge zone because the turbulent Schmidt number $S_c \equiv v_t / K_y$ becomes almost one.
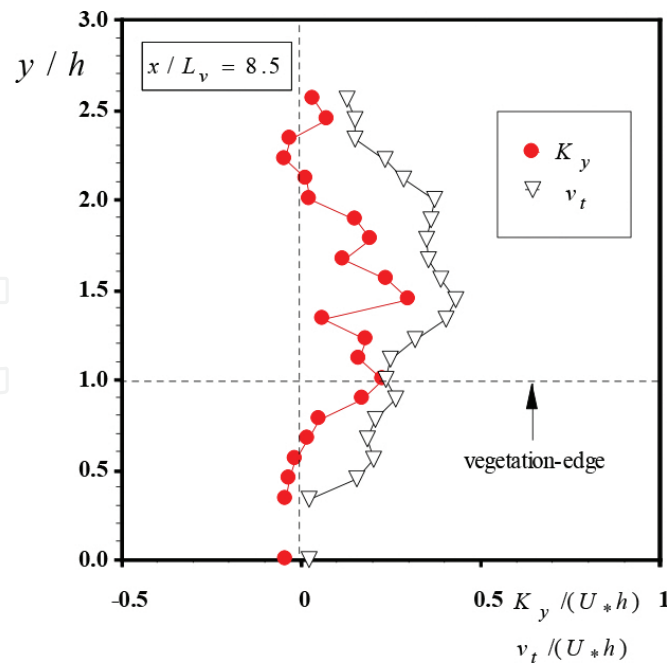
Figure 21. Vertical profiles of turbulence diffusivity and eddy viscosity.

4. Conclusions

The Section 2 explained the PIV turbulence measurements and their results in the vegetated open-channel flows. Particularly, mean-flow properties, turbulence structure, and coherent motions were revealed as follows;

1. In the larger submergence depth condition, the momentum transfer of Reynolds stress toward the within canopy layer is promoted significantly. Consequently, the penetration depth is evaluated reasonably from the Reynolds stress distributions. On the basis of mean velocity profiles and the eddy periodicity, it was found that there is a significant analogy between the canopy shear layer and the mixing shear layer.

2. The coherent eddy has a significant relation with generations of the sweeps and the ejections, and the trajectory of the vortex core is driven by these coherent motions. The length scales of coherent eddies were evaluated from PIV images, and it was found that the large-scale eddies appear in large submergence depth.

The Section 3 introduced PIV and LIF simultaneous measurement technique with two sets of high-speed cameras, which could evaluate the relation between the turbulent diffusion property and coherent motions. The main findings obtained here are as follows;

1. Two components of the instantaneous velocity vectors and the dye concentration were measured simultaneously using the combination of PIV and LIF methods. The dye concentration is lifted up to the over-canopy by the ejection motions, and returned to the within-canopy by the sweep motion.

2. The contribution of the sweep motion to the transport of the dye concentration is larger than that of the ejection motions near the vegetation edge, and it was found from the simultaneous measurements of the velocity and concentration that the turbulent diffusivity is in the same order of magnitude as the eddy viscosity.

Author details

Michio Sanjou

Address all correspondence to: michio.sanjou@water.kuciv.kyoto-u.ac.jp

Department of Civil and Earth Resources Engineering, Kyoto University, Kyoto, Japan

References

[1] Raupach, M. R. and Thom, A. S.: Turbulence in and above plant canopies. Ann. Rev. Fluid Mech. 1981;13:97–129.

[2] Gao, W., Shaw, R. H. and Pawu, K. T.: Observation of organized structure in turbulent flow within and above a forest canopy turbulent in and above plant canopies. Bound. Layer Meteorol. 1989; 47: 349–377.

[3] Raupach, M. R., Finnigan, J. J. and Brunet, Y.: Coherent eddies and turbulence in vegetation canopies: the mixing-layer analogy. Bound. Layer Meteorol. 1996; 78: 351–382.

[4] Nepf, H. M., Sullivan, J. A. and Zavistoski, R. A.: A model for diffusion within emergent vegetation. Linnol. Oceanogr. 1997; 42(8): 1735–1745.

[5] Nepf, H. M.: Drag, Turbulence, and diffusion in flow through emergent vegetation. Water Resour. Res. 1999; 35: 479–489.

[6] Poggi, D., Porpotato, A. and Ridolfi, L.: The effect of vegetation density on canopy sublayer turbulence. Bound. Layer Meteorol. 2004; 111: 565–587.

[7] Ghisalberti, M. and Nepf, H.: The structure of the shear layer in flows over rigid and flexible canopies. Environ. Fluid Mech. 2006; 6: 277–301.

[8] Nepf, H. M. and Vivoni, E. R.: Flow structure in depth-limited vegetated flow. J. Geophys. Res. 2000; 105: 28547–28557.

[9] Nezu, I. and Nakagawa, H.: Turbulence in open-channel. IAHR Monogr. Balkema. 1993.

[10] Wilson, C. A. M. E, Stoesser, T., Bates, P. D. and Batemann Pinzen, A.: Open channel flow through different forms of submerged flexible vegetation. J. Hydraul. Eng. 2003; 129: 847–853.

[11] Ho, C. M. and Huerre, P.: Perturbed free shear layers. Ann. Rev. Fluid Mech. 1985; 16: 365–424.

[12] Adrian, R. J., Meinhart, C. D., Tomkins, C. D.: Vortex organization in the outer region of the turbulent boundary layer. J. Fluid Mech. 2000; 422: 1–54.

[13] Komori, S., Nagaosa, R. and Murakami, Y.: Turbulence structure and mass transfer across a sheared air–water interface in wind driven turbulence. J. Fluid Mech. 1983; 249: 161–183.